JOURNAL OF MATERIALS SCIENCE 26 (1991) 1497–1504

Surface contamination and its effect on the corrosion of rapidly solidified Mg–Al alloy splats

C. B. BALIGA*, P. TSAKIROPOULOS*, C. JEYNES‡
* *Department of Materials Science and Engineering and* ‡ *Department of Electrical and Electronic Engineering, University of Surrey, Guildford, Surrey GU2 5XH, UK*

Contamination with copper particles of the surfaces of rapidly solidified Mg–3.5 wt% Al alloy splats during processing is discussed. Two batches of splats produced with copper substrates of different surface finish, were examined by atomic absorption spectrometry (AAS), electron probe micro-analysis (EPMA) and Rutherford back scattering (RBS). Lower copper content was detected on the well-polished splats (splats B) by AAS, while EPMA and RBS analysis with a micro-beam showed fine copper particles on the surfaces of the splats prepared with pistons of inferior surface finish (splats A). Immersion corrosion tests carried out in a 3% NaCl solution saturated with $Mg(OH)_2$ resulted in higher pit density and earlier pitting times for splats A. Pitting is associated with copper particles (splats A) and with surface cracks and macro-porosity (splats A and B). A mechanism for pitting is suggested in which Mg(OH)Cl is envisaged to be an intermediate reaction product before decomposing to $Mg(OH)_2$ in the pitting process.

1. Introduction

The corrosion performance of magnesium and its alloys in a saline environment is greatly affected by metallic impurities, which can overshadow the effects of flux inclusions, nonmetallic impurities, porosity and grain size [1, 2]. Chemical pickup of heavy metal contamination during casting operations of magnesium and its alloys has been extensively observed and reported in the literature [1, 2, 3]. With the advent of rapid solidification (RS) processing the deleterious effects of heavy metal contamination in such alloys have been greatly reduced. Furthermore, RS processing has improved the corrosion resistance of magnesium alloys by achieving homogeneous distribution of such metallic and nonmetallic impurities [4].

RS processing of magnesium and its alloys has been carried out by gas atomization, melt extraction or melt spinning and splat quenching [5], each method having its own merits with regard to melt capacity, production rates and cooling rates. From all previous methods the highest quenching rates have been achieved by the splat quenching techniques, where copper pistons are usually employed as quenching substrates. This paper addresses the problem of heavy metal contamination (copper) during the splatting process. The effect of these copper particles on pitting corrosion is also discussed.

2. Experimental procedure

Splats of Mg–3.5 wt % Al were prepared under argon using the twin piston quenching technique with copper pistons. The Mg–3.5 wt % Al ingot was supplied by Magnesium Elektron Ltd, (MEL). The splats were produced by levitation melting 100 mg specimens in a preparation chamber filled with argon. Subsequent handling was done under argon with short exposures to air during the transfer of the specimens to various instruments. The surfaces of the splats were examined by optical and scanning electron microscopy (SEM), electron probe micro-analysis (EPMA) and Rutherford backscattering spectrometry (RBS). Standard specimen preparation techniques were used for SEM, EPMA and RBS [6, 7, 8]. The microstructure of splats was examined by transmission electron microscopy (TEM). TEM specimen preparation has been described elsewhere [9].

Immersion corrosion tests were carried out in a 3% NaCl solution saturated with $Mg(OH)_2$ [8] at 20 °C for different lengths of time, from 0 to 150 min with time intervals of 1, 2, 4, 5, 10, 15, 30, 45, 60, 90, 120 and 150 min. Corroded splats were carefully handled using clean plastic tweezers, and dried in air after draining the excess solution on to a tissue paper [9]. For comparison purposes some corroded splats were also washed in distilled water and dried in argon. The surfaces of the immersed splats facing upwards were examined under the different techniques mentioned earlier.

EPMA was carried out on a Jeol 35CF with oxygen analysis using a windowless technique. A Cambridge Stereoscan 250 was used to study the surface morphology of the splats. RBS was carried out with a focused beam of 1.5 MeV $^4He^+$ ions scattered

0022–2461/91 $03.00 + .12

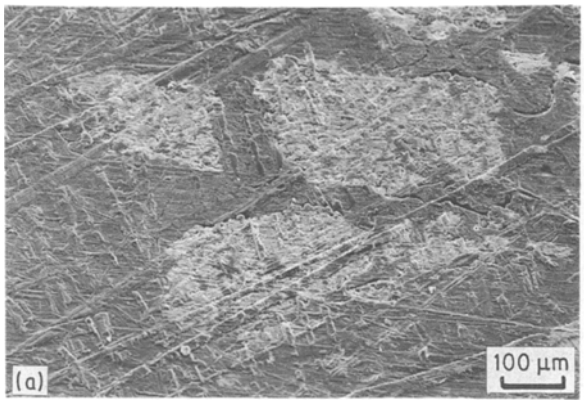

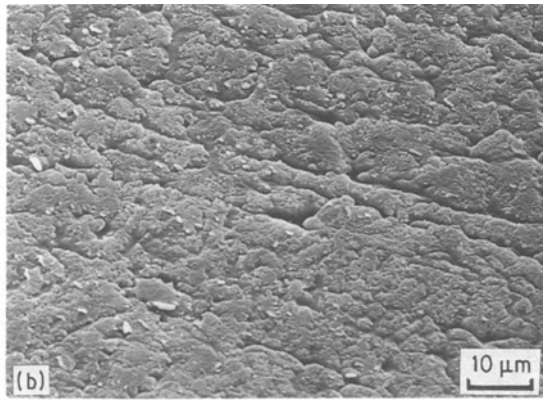

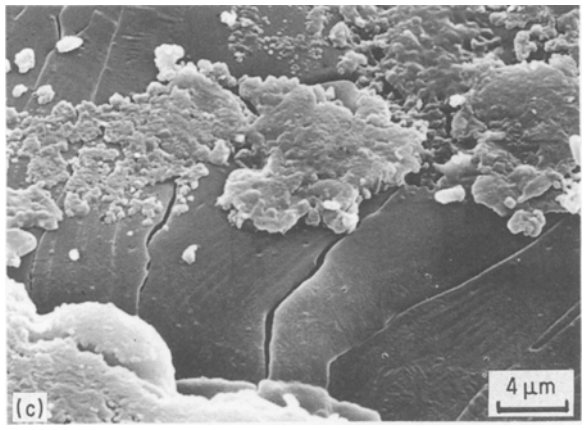

Figure 1 SEM micrographs showing the typical surface morphology of Mg–3.5 wt % Al splats; (a) hills and valleys corresponding to polishing lines on the copper pistons and islands of high temperature oxide; (b) rifts; (c) high temperature oxide (formed during levitation melting and retained on the surface of the splat [9]) covering a surface crack.

through 165°. The experimental arrangement has been described previously [10]; briefly an objective aperture of 200 μm or 50 μm was used to define the beam, and a Russian quadruplet of quadrupole magnets formed an image of the aperture with 5 × demagnification on the splat surface. The beams could be scanned over about 1 mm on the sample without excessive spherical aberration by pairs of opposed electrostatic scanning plates which rock the beam about the optical centre of the quadruplet. Standard spectrometry electronics and data analysis were used [7] as well as standard energy loss data [11] to obtain depth scales from the energy analysis spectra.

3. Results

3.1. Characterization of splats as received

Two batches of about 30 splats each were produced using material from the ingot supplied by MEL. The same conditions were kept for both batches with the exception that for batch I (splats A) the copper pistons were polished with wet emery paper and finished with grade No. 800 and for the second batch (splats B) the finer 1/4 μm diamond finish was used. In the latter case the pistons were also repolished after a set of ten splats was produced. At least five splats from both batches were selected randomly and were analysed by AAS for Cu, Fe, Mn, Ni, Pb and Zn. The analysis results are given in Table I.

The surfaces of the splats were examined under the SEM. Fig. 1a shows the typical general morphology of these surfaces. Hills and valleys corresponding to scratches on the surfaces of the pistons are clearly seen. These features were more pronounced on splats A. In addition, cracks (Fig. 1a) and rifts (Fig. 1b) were also present. On the surfaces of splats A small particles of copper were identified (Fig. 2a) whose size varied from 1 to 10 μm in diameter although finer particles with diameter less than 1 μm could also be detected at higher magnifications (> 5000 ×, Fig. 2c). Because of their size, the distribution and exact location of these particles could not be assessed accurately. These particles were subsequently analysed by EPMA and RBS. In the former case dot maps were used for their identification (Fig. 2b). RBS confirmed that the particles were on the surface.

EPMA provides a good elemental specificity and lateral resolution. The drawback of this technique is that the X-ray signal reflects the average compositions over depths large compared to the depth resolution of a backscattering spectrum. Fig. 3 is a typical backscattering spectrum from a Mg–3.5 wt % Al splat with copper particles using a 50 μm beam and shows that copper is present at the surface oxide of the splat. The magnesium surface signal indicated a strongly varying oxygen content with depth: this is consistent with X-ray photoelectron spectroscopy (XPS) depth profiling [9] and can be attributed to a size distribution of oxide particles with maximum particle size around 140 nm. The surface concentration of copper in the spectrum is approximately 0.3 at % (± 10 %) which corresponds to a 2 μm copper particle at the surface. The large oxygen signal indicates the presence of an oxide with an estimated stoichiometry at the surface of approximately Mg_4O_3. This corresponds to oxide particle/s covering 3/4 of the surface (see also Fig. 1c). The lead concentration in the bulk as estimated from

TABLE I Chemical analysis of Mg–3.5 wt % Al alloy splats

Alloy	Impurities analysed by Atomic Absorption Spectroscopy (in p.p.m.)					
	Cu	Fe	Ni	Zn	Pb	Mn
Splats A	110	50	< 10	90	< 100	80
Splats B	< 50	< 50	< 30	70	< 80	70

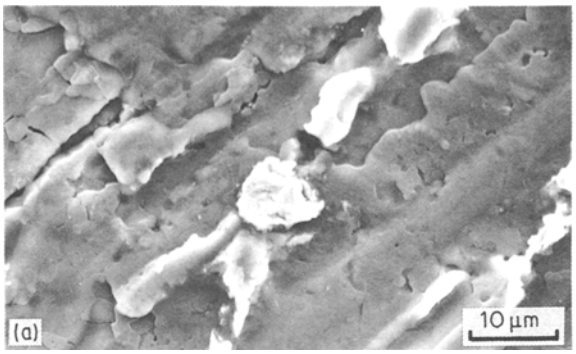

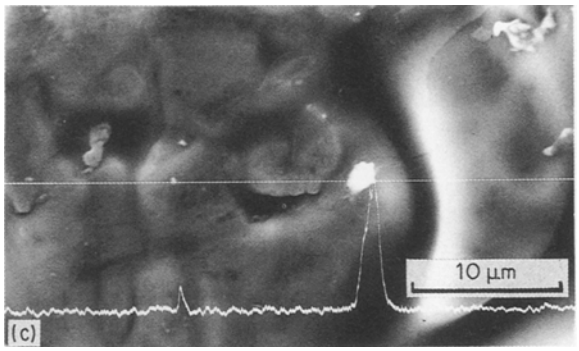

the spectrum in Fig. 3b is approximately equal to 30 p.p.m.

The grain size, determined by TEM, varied from 1 to 5 μm in both sets of splats (Fig. 4). Some grains exhibited an aspect ratio of two with a high dislocation density within the grains [9]. The grain boundaries and grain interiors were free from precipitates.

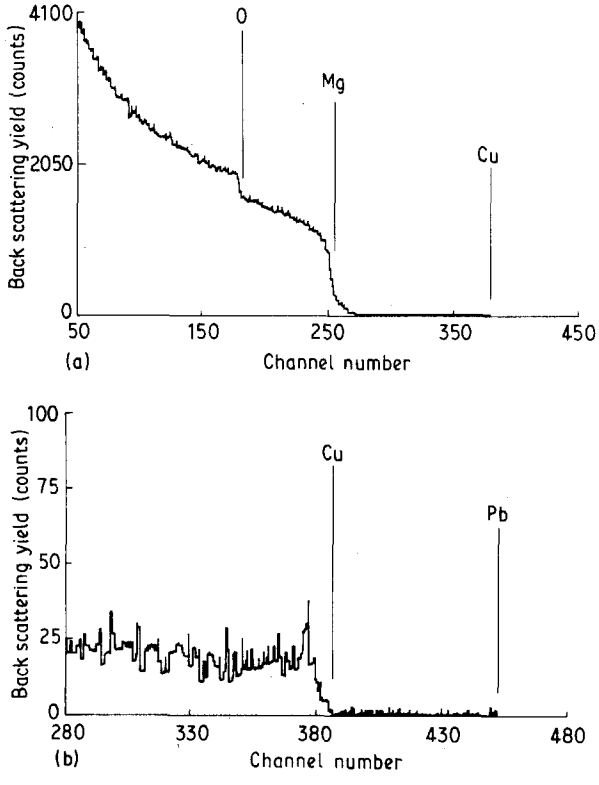

Figure 3 RBS spectra of a typical Mg–3.5 wt % Al splat (splats A), using a 1.5 MeV beam with a 165° scattering angle, (a) indicating the presence of copper particles on the surface of the splat and (b) a detailed region near the copper edge.

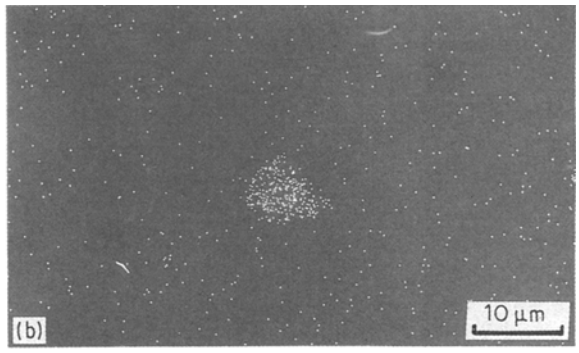

Figure 2 SEM micrographs showing copper particles on the surface of a Mg–3.5 wt % Al splat (splat A); (a) copper particle (indistinguishable); (b) Cu$K\alpha$ dot map of (a); (c) line trace of the copper particles.

3.2. Characterization of corroded splats

During immersion in the corrosive environment, gas (hydrogen) evolution could be detected from the surface of splats A and B. Rigorous hydrogen gas evolution was observed in certain areas on splats A. On the contrary, on splats B the gas evolution occurred more or less uniformly from all over the surface.

Localized attack occurred during the corrosion tests which resulted in perforation of the splats of both batches. Here we refer to perforation as pitting. The pits had a diameter which was less than 500 μm for splats A and 200 μm for splats B. The number of pits was measured from montage of optical micrographs taken from the corroded splats. The former splats had 16×10^4 pits m^{-2} as compared with 7×10^4 pits m^{-2} in the splats B.

Localized (as observed by optical microscopy and SEM) attack on splats A started after 60 min and after 100 min for splats B, and pitting (determined by the formation of perforations) occurred after 120 min and 150 min, respectively. Regions of localized attack were associated with Cu particles in the case of splats A (Figs 5 and 6), and with surface cracks [9] and porosity (Fig. 7) for both splats A and B. The corrosion product on and around the pits eventually grew into a voluminous product (Fig. 8). At higher magnifications however a fine needle like acicular overgrowth structure (Fig. 9) could be seen in both washed and unwashed specimens. The fine needle like structure

Figure 4 TEM micrograph of Mg–3.5 wt % Al splat showing fine grain size microstructure.

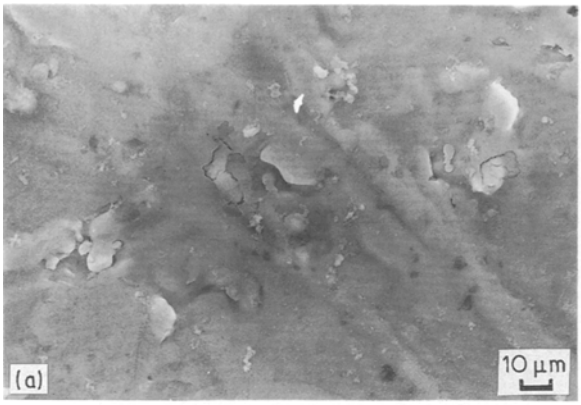

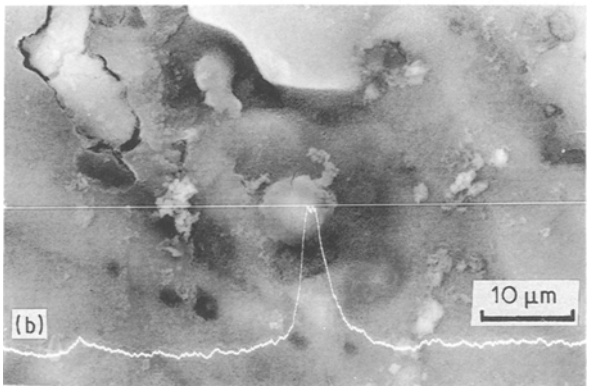

Figure 5 SEM micrographs of a Mg–3.5 wt % Al splat (splats A) showing localized attack near the polishing lines of the splat after 15 min in 3% NaCl solution saturated with $Mg(OH)_2$; (a) low magnification; (b) higher magnification of (a).

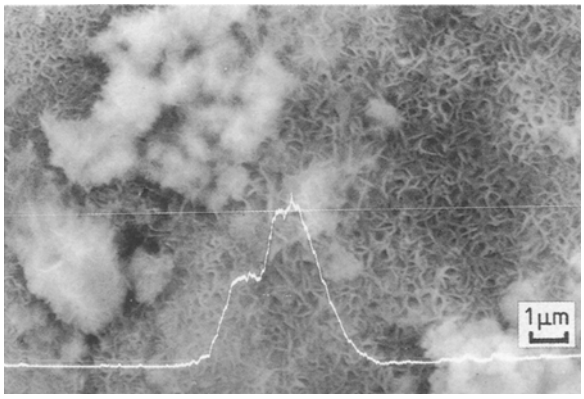

Figure 6 SEM micrograph showing corrosion products of acicular structure around copper particles on a Mg–3.5 wt % Al splat (splats A) in 3% NaCl solution saturated with $Mg(OH)_2$, (15 min).

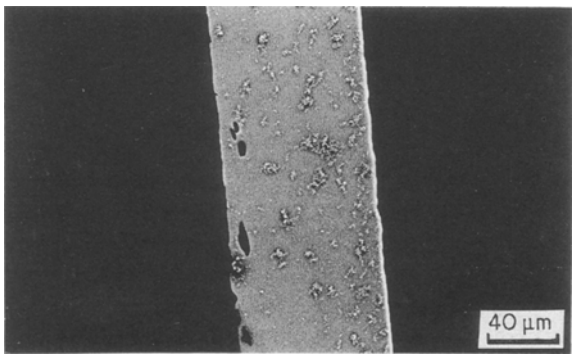

Figure 7 SEM micrograph showing porosity in a Mg–3.5 wt % Al splat (backscattered image).

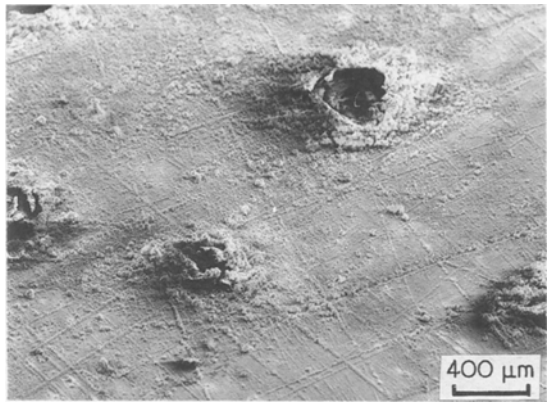

Figure 8 SEM micrograph of a Mg–3.5 wt % Al splat corroded in 3% NaCl solution saturated with $Mg(OH)_2$ for 150 min at 20 °C showing the surface morphology around a pit.

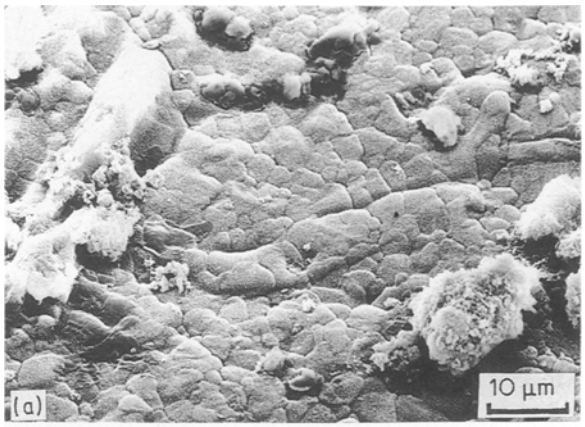

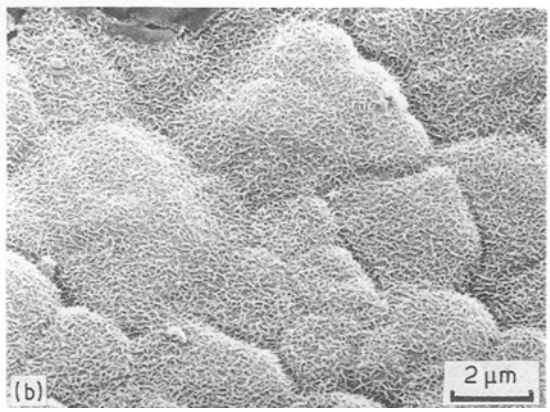

Figure 9 SEM micrographs of a Mg–3.5 wt % Al splat corroded for 90 min in 3% NaCl solution saturated with $Mg(OH)_2$ at 20 °C showing the surface morphology of "unaffected" regions; (a) low magnification; (b) higher magnification.

evolved into one of coarser needles and plates as the time of exposure in the corrosive environment was increased (Fig. 10). The acicular structure identified as $Mg(OH)_2$ and/or hydromagnesite [9] was associated with rifts or wide shallow valleys on the surface.

Concurrently with the coarsening of the fine needles and the appearance of plates (Fig. 10) preferred growth of the acicular corrosion product occurred at certain locations. Sometimes these were associated with copper particles (Fig. 6), resulting in isolated caps of the acicular corrosion product. Growth of the

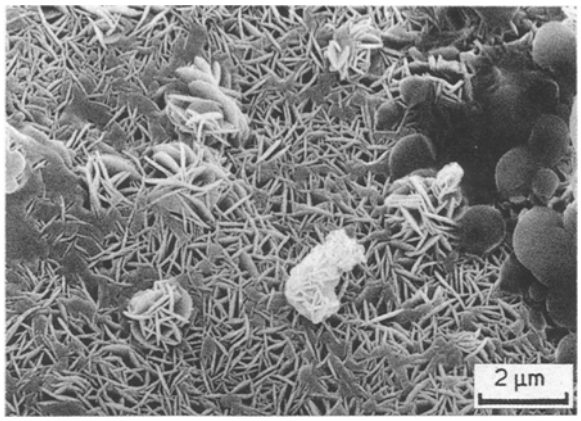

Figure 10 SEM micrograph of a Mg–3.5 wt % Al splat corroded for 150 min in 3% NaCl solution saturated with $Mg(OH)_2$ at 20 °C showing $Mg(OH)_2$ platelets.

voluminous product was more pronounced near the edges of the splats where platelets could be seen on the surface. EPMA analysis of the corrosion product indicated Mg, O, Al, Cl and Na with the oxygen level increasing with exposure time and eventually reaching levels having a peak intensity almost equal to that of magnesium after 17 h (Fig. 11). At this exposure time the whole surface of the splats was covered with corrosion product and the splats became extremely brittle. Sodium was adsorbed on the surface as shown by XPS [9].

The RBS spectrum (Fig. 12) from splats corroded for 150 min (the pitting time) showed an average composition approximately MgO_2 (hydrogen is not analysed here) with a Cl:Mg ratio rising from 1:6 to 1:3 at the surface. A similar analysis carried out on highly corroded splats (after 645 min) showed a similar average composition, approximately MgO_2, but the Cl:Mg ratio was about 1:9 rising to 1:6 near the surface. There was a Cl–rich surface layer about 100 nm thick in both the cases.

4. Discussion

The pitting density (perforation density) of splats A was higher by 2.3 times that for splats B. This is in agreement with the results of another study [12] where the corrosion rates of splats prepared following the same procedure as for splats A were found to be twice those of splats prepared similarly to our splats B. Furthermore, RBS has shown higher concentration of copper on the surface of splats A than in the bulk. Chemical analysis by AAS (Table I), though close to the detection limits of the technique, has also indicated a higher copper content in them than in splats B. For all other elements their concentration was well within the expected concentration limits [13]. For both

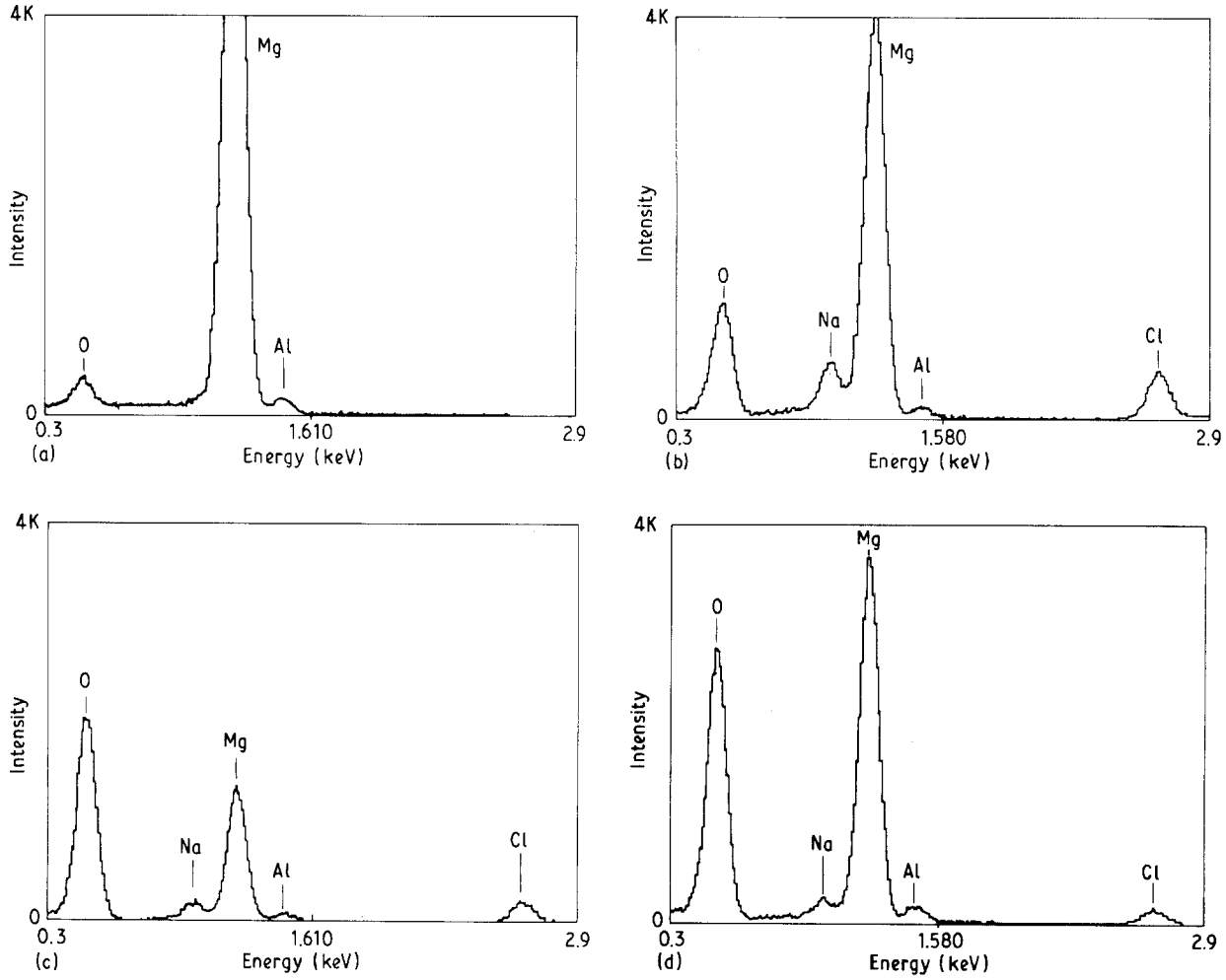

Figure 11 Montage of windowless EDX analysis of Mg–3.5 wt % Al splats corroded in 3% NaCl solution saturated with $Mg(OH)_2$ for different lengths of time at 20 °C; (a) as-received; (b) 90 min; (c) 150 min; (d) 17 h.

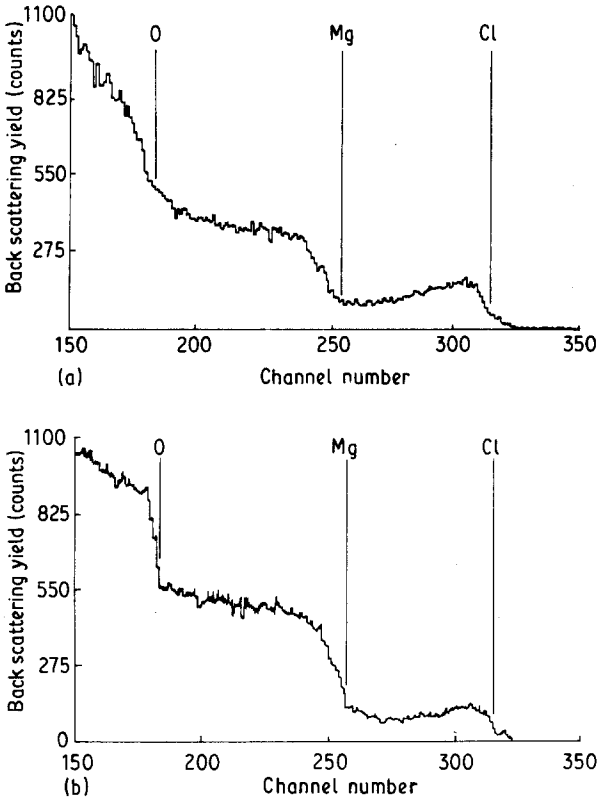

Figure 12 RBS spectra using 1.5 MeV with a 165° scattering angle, of Mg–3.5 wt % Al splat, corroded in 3% NaCl solution saturated with $Mg(OH)_2$ showing depletion of chlorine with depth (decreasing channel number); (a) after 150 min; (b) after 645 min. In (a) the edge corresponds to chlorine isotope.

batches of splats the microstructure was a solid solution, as expected from the phase diagram [14]. The TEM micrographs of the splats showed no differences with respect to grain size and grain boundary characteristics. Therefore, the microstructure of the splats cannot be considered responsible for the difference in pitting behaviour of splats A as compared with splats B.

The higher pitting densities of splats A are correlated with the presence of detritous fine copper particles. The sources of these particles are the copper pistons used as quenching substrates. Copper pick-up on the surfaces of melt-spun Al–Mn and Al–Fe ribbons has also been reported when the melt was ejected on to a rotating copper wheel [15].

Three types of regions have been identified on the surface of the splats, where attack having once started became self-sustaining. These are: (i) fine Cu particles at the surface (splats A); (ii) cracks (including the specimen edges); and (iii) macro-porosity connected with the surface of the splats, the latter two occurring in both splats A and B.

4.1. Corrosion mechanism

Copper, like most metals, is cathodic (more noble) to magnesium. Thus the degree to which the corrosion of magnesium is accelerated under the given conditions depends on how rapidly the effective potential of the Cu/Mg couple is reduced by polarization as galvanic current flows. The main polarization mechanism, in any magnesium couple in a NaCl solution, is the resistance to the formation and liberation of hydrogen gas at the cathode. Copper, a metal of low hydrogen overvoltage, will thus constitute an efficient cathode for magnesium and would cause severe galvanic corrosion. This is consistent with the observation of vigorous gas evolution from certain areas of the surfaces of splats A.

Following Tomashov *et al.* [16], Robinson and King [17, 18] and Wranglen [19], we postulate that initiation of pits generally occurs by adsorption of activating anions (Cl^-) on certain defective sites (e.g., kinks, voids) in the $MgO/Mg(OH)_2$ overgrowth film [9]. Under the influence of the corrosion current generated by the pit cell, migration of chloride ions occurs inside the pit causing enrichment in chloride ions. Simultaneously an acid solution within the pit is produced by hydrolysis of metal ions. This results in a highly concentrated conductive salt solution having a low solubility of dissolved oxygen which in turn accelerates pitting. Presence of noble metals (Cu in our experiment) in the vicinity of the pits maintains the cathodic potential, thus again facilitating pitting. Furthermore, the generation of hydrogen ions and chlorine ions lowers the pH at the bottom of the pit and consequently the dissolution rate of Mg is increased. This increase in dissolution increases migration and the result is the self-sustaining pitting attack.

In a vicious circle the pit creates conditions which promote its further growth. This is evident from the pitting times and the number of pits observed for the splats A and B.

The above mechanism is explained schematically in Fig. 13. The anodic metal dissolution reaction at the bottom of the pit

$$Mg \rightarrow Mg^{2+} + 2e^- \quad (1)$$

is balanced by the cathodic reaction on the adjacent surface

$$O_2 + 2H_2O + 4e^- \rightarrow 4(OH)^- \quad (2)$$

The increased concentration of Mg^{2+} within the pit will then cause migration of Cl^- to maintain neutrality and is hydrolysed by water as

$$Mg^{2+} + H_2O + Cl^- \rightarrow Mg(OH)Cl + H^+ \quad (3)$$

$$2H^+ + 2e^- \rightarrow H_2\uparrow \quad (4)$$

$$Mg(OH)Cl + H_2O \rightarrow Mg(OH)_2\downarrow + H^+ + Cl^- \quad (5)$$

$$Mg + 2H_2O \rightarrow Mg(OH)_2\downarrow + H_2\uparrow \quad (6)$$

The above mechanism is also true for pits initiated on surface cracks [9] as well as on macro-pores connected with the surface *via* a narrow entry (Fig. 7).

RBS analysis after different corrosion times of 150 min and 645 min (Fig. 12a, b) has indicated a very high chlorine concentration at the surface at a pitting time of 150 min, while after longer exposures (645 min) the chlorine concentration remained at high levels. EPMA results also showed a similar trend (Fig. 11). Chlorine plays a major role in the pitting process and after pit initiation a uniform chlorine attack is observed.

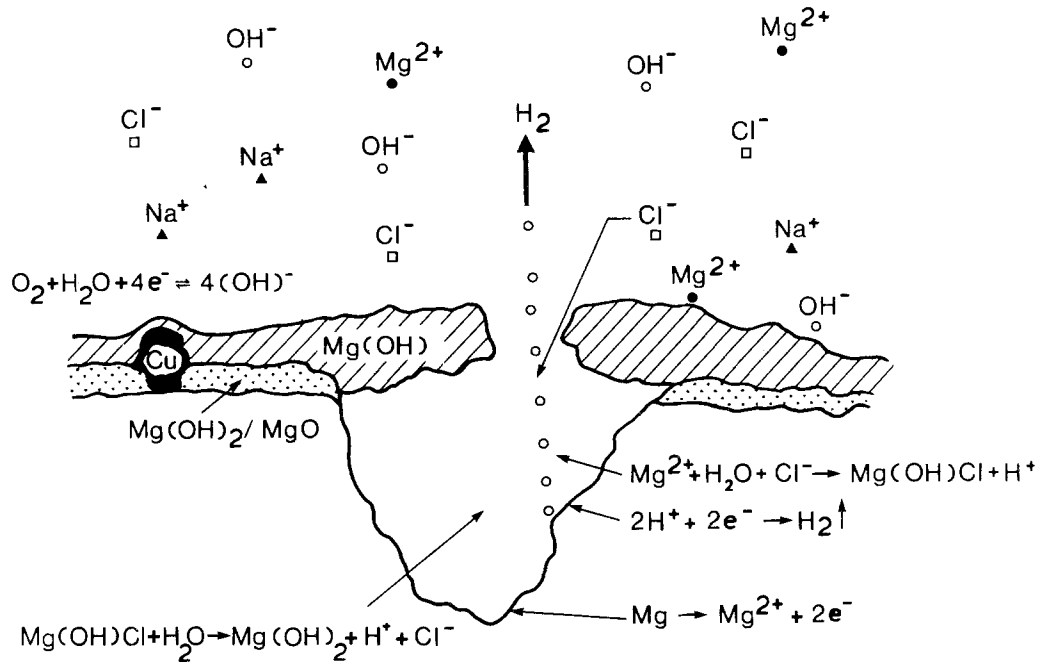

Figure 13 Schematic of the mechanism of localized attack of Mg–3.5 wt % Al splats.

Robinson and King [17] have reported that in NaCl electrolytes magnesium hydroxy-chloride occurred as a corrosion product, even at low anodic currents. Formation of Mg(OH)Cl has also been postulated by Casey and Bergeron [20]. It is proposed that Reactions 1 and 3–5 are possible intermediate reactions in the acidic environment in the pit and lead to the formation of Mg(OH)Cl. The presence of Cl^- and $(OH)^-$ on the surfaces of the corroded splats has been confirmed by XPS [9]. Depth profiling by argon ion sputtering indicated decreasing levels of Cl^- and $(OH)^-$ on the surfaces of both washed and unwashed specimens [9]. These results, together with the determination of chlorine by RBS on the surfaces of the corroded splats provide further indirect evidence of the formation of Mg(OH)Cl as an intermediate corrosion product (Reaction 3 above) which then dissociates to give $Mg(OH)_2$ according to Reaction 5. The presence of the insoluble hydroxide, $Mg(OH)_2$, is in agreement with the EPMA and RBS results indicating the increased oxygen content on the splat surface with increased exposure time to the corrosive environment and with the presence of MgO and $Mg(OH)_2$ in the surfaces of corroded splats as reported in [9].

Once a pit is initiated in any of the three locations discussed above, its propogation is very dependent on hydrogen ion concentration and accumulation of chloride ions in the pit. The decrease of pH in the pit cavity will promote more rapid anodic dissolution of its surface. The geometry of macro-pores such as those in Fig. 7 is expected to be essential in promoting electrochemical heterogeneity since their interior functions as an anode and their exterior as a cathode. Considerable potential gradient is caused by the high resistance of the narrow electrolytic path which prevents the passivation of the pore interior. Central porosity has also been identified in the splats (Fig. 7). Although initially these pores are not connected with the surface, once pits have started to become deeper, these central pores will eventually come in contact with the corrosive environment and attack will be accelerated over a larger area by the mechanism discussed previously. The presence of pores is therefore detrimental for the pitting corrosion and care should be applied when assessing the corrosion results for RS alloys using splats as specimens for the evaluation experiments.

5. Conclusions

The corrosion of Mg–3.5 wt % Al splats, prepared by the twin piston quenching technique with the Cu pistons, is affected by the presence of copper particles on the surface of the splats. Such surface contamination could mislead the assessment of the corrosion resistance of an alloy. Therefore, special care is required during the processing of magnesium alloys by this (and other) rapid solidification technique.

Chlorine ions are instrumental in damaging the prior oxide and/or hydroxide present on the surface of the splats. Pitting of the splats is attributed to the formation of local anodic and cathodic areas due to surface non-uniformity (roughness), porosity and variable oxide/hydroxide film thickness. Mg(OH)Cl is envisaged to be an intermediate reaction product in the pitting process and to decompose to $Mg(OH)_2$.

6. Acknowledgement

The authors would like to thank Professor J. E. Castle for the provision of research facilities in the Department of Materials Science and Engineering and thank Professor H. Jones (University of Sheffield) for the provision of the splats. C.B.B. would also like to acknowledge the financial support rendered by ALPOCO, Magnesium Electron Ltd, and Shell Research Ltd.

References

1. K. N. REICHEK, K. J. CLARK and J. E. HILLIS, SAE Technical Paper, No. 850417, March, 1985.
2. J. D. HANAWALT, C. E. NELSON and J. A. PELOUBET, *Trans. Amer. Inst. Mining Met. Eng.* **147** (1942) 273.
3. E. F. EMLEY, in "Principles of Magnesium Technology" (Pergamon Press, New York, 1966).
4. R. E. LEWIS, A. JOSHI and H. JONES, Proceedings of the International Conference on Enhanced Properties of Structural Materials via Rapid Solidification, Orlando, Florida, Oct. 4–9, 1986 (ASM, Metals Park, Ohio) p. 367.
5. F. HEHMANN and H. JONES, in "Magnesium Technology" (The Institute of Metals, London, 1986) p. 83.
6. METALS HANDBOOK, 9th Edn, Vol. 10, Material Characterization (ASM, Ohio, 1986) pp. 568, 628.
7. W.-K. CHU, J. W. MAYER and M. A. NICOLET, in "Backscattering Spectrometry" (Academic Press, New York, 1978).
8. E. F. EMLEY, A. C. JESSUP and W. F. HIGGINS, *J. Inst. Metals* **80** (1951–52) 23.
9. C. B. BALIGA, P. TSAKIROPOULOS and J. F. WATTS, **4** (1989) 231.
10. A. P. MATTEWS, C. JEYNES, K. J. RUSON and J. THORNTON, *Nuclear Instr. Methods* **330** (1988) 497.
11. J. F. ZIEGLER, in "Helium stopping powers and ranges in all elemental matter" (Pergamon Press, NY, 1977).
12. D. S. AHMED, University of Sheffield, unpublished work.
13. W. UNSWORTH, MEL, private communication.
14. J. L. MURRAY, *Bull. Alloy Phase Diagrams* **3** (1982) 60.
15. A. CSANADY, I. BETROTI, M. MOHAI, S. PEREEL and B. ALBERT, *Surface Interface Analysis* **12** (1988) 229.
16. N. D. TOMASHOV, V. S. KOMISSAROVA and M. A. TIMONOVA, *Issledoran Korrozi Metal, No.* 4 (1985) 172.
17. J. L. ROBINSON and P. F. KING, *J. Electrochem. Soc.* **108** (1961) 36.
18. P. F. KING, *ibid.* **113** (1966) 536.
19. G. WRANGLEN, in "An introduction to corrosion and protection of metals" (Chapman and Hall, London, 1985).
20. E. J. CASEY and R. E. BERGERON, *Canadian J. Chem.* **31** (1953) 849.

Received 16 June
and accepted 19 October 1989